DEUTSCHES ELEKTRONEN-SYNCHROTRON DESY

THE ARGUS ELECTRON-PHOTON CALORIMETER

III.   ELECTRON-HADRON SEPARATION

by

A. Drescher, B. Gräwe, B. Hahn, B. Ingelbach, U. Matthiesen,

H. Scheck, J. Spengler and D. Wegener

Institut für Physik, Universität Dortmund

NOTKESTRASSE 85 · 2 HAMBURG 52

To be sure that your preprints are promptly included in the
HIGH ENERGY PHYSICS INDEX ,
send them to the following address (if possible by air mail) :

DESY
Bibliothek
Notkestrasse 85
2 Hamburg 52
Germany

The ARGUS Electron-Photon Calorimeter

III) Electron-Hadron Separation

A. Drescher, B. Gräwe, B. Hahn, B. Ingelbach, U. Matthiesen,
H. Scheck, J. Spengler and D. Wegener

Institut für Physik
Universität Dortmund

Abstract:

The high granularity of the ARGUS shower counter system allows
one to determine the lateral energy deposition. An algorithm
based on the number of shower counters set by an incoming particle,
the amount of energy deposited in the shower counters and the
lateral distribution of the energy allows to separate electrons
from muons and hadrons. For electrons with momenta larger than
0.7 GeV/c the hadron rejection rate is of the order of 50 at an
electron detection efficiency of 80%.

I. Introduction

The ARGUS spectrometer (fig. 1) is a detector for e^+ e^- reactions
at DORIS II [1]. It consists of a central drift chamber [2], which
measures the momentum of charged particles and the rate of their
energy loss, a time of flight system [3] and an electromagnetic
shower detector [4]. These components are all inside of the coil
of the magnet, which produces a nearly homogeneous field of 0.8 T.
Muons are detected in two planes by proportional tubes [5], positioned
behind absorbers, with cut off momenta of 0.7 GeV/c and 1.1 GeV/c
respectively.

Details of the performance of the shower counters in a test beam
and under experimental conditions in the ARGUS detector have been
previously described [4]. In this paper we will concentrate on the
question of how electrons (used as a synonym for electrons and
positrons) can be separated from other charged particles hitting
the shower counters. A clean electron sample, identified with high
efficiency and with a small hadron admixture, is of interest
for the physics program performed with the ARGUS detector, namely
the study of semileptonic B decays. These can be used to determine
the branching ratios BR(b→c) and BR(b→u), as well as to search
for B^0-B^0 mixing. For these physics goals, the electron momentum
range of main interest is 1.2 GeV/c $\leq P_e \leq$ 2.5 GeV/c.

Contrary to most other experiments [6,7] the separation of
electrons and hadrons has to be based entirely on the differences
of the lateral energy deposited by particles hitting the shower
counters, because there is only one longitudinal sample.
Since the lateral width of the shower counters, r ≈ 10 cm, is large
compared with the radius of a typical electromagnetic shower
(Moliere radius R_M <5 cm) but is small in comparison with the radius
of a hadronic shower (absorption length λ_{abs} ≈ 46 cm), the two kinds
of showers can be distinguished. On the other hand minimum ionizing
particles can be separated from showering electrons, simply on the
basis of the energy deposited.

The paper is organized as follows: in section II we briefly describe those properties of the ARGUS electron photon calorimeter, which are of importance for the present analysis. Further details have been given in previous publications [4]. In section III the pattern of energy deposition for the different particles species is discussed. In section IV we describe the algorithm which exploits the results of section III with the aim of electron hadron separation at different momenta.

II. ARGUS electromagnetic calorimeter

The ARGUS shower counters are of the lead scintillator sandwich type with 5 mm thick scintillator plates (Altustipe UV). The thickness of the lead plates is 1 mm in the barrel, and 1.5 mm in the endcap region. The overall length of each counter corresponds to 12.4 radiation lengths for electrons and 0.8 absorption lengths for pions in the momentum range of interest. The lead and scintillator plates are separated by aluminized mylar foils with 98% reflectivity. The lead scintillator sandwich is "read out" by a 3 mm thick wave length shifter coupled to a 1 inch photo tube (Valvo XP 2008 UB). The barrel counters consist of 64 plates of each material with 10.9 cm x 10.3 cm lateral cross section. The endcap counters contain 45 plates of each material of trapezoidal shape with maximum lateral dimensions of 11.6 cm and 10.4 cm.

The shower counters are mounted inside of the magnetic coil. The cylindrical arrangement of the barrel counters (fig. 1) results in a variation of the angle of incidence between 0° and 45° for particles coming from the interaction point. The endcap counters are arranged in a plane perpendicular to the primary beam (fig.1), the angle of incidence for particles hitting this detector component varies between 20° and 45°. Because of the cylindrical symmetry of the detector counters in the same polar angle region can be treated in common. Counters at $\theta = 90°$ are labelled with the ring number 1, with decreasing polar angle the ring number increases to 15 for the counters in the endcap at the smallest polar angles.

The energy resolution presently obtained under experimental conditions is

$$\frac{\sigma}{E} = \sqrt{(\frac{0.08}{\sqrt{E}})^2 + (0.068)^2}$$

where E is measured in GeV.

The angular resolution is 0.7° for electrons with momenta $p_e \geq 1$ GeV/c. Further details concerning the construction and properties of the shower counters are described in ref. [4b,c,d].

III. Pattern of energy deposition for different particle species

The following information about the energy deposited by a particle in the ARGUS shower counters is available: the total visible energy deposited, E, the number of neighbouring counters hit (cluster size, n) and the visible energy E_i detected in each counter of a cluster:

$$E = \sum_1^n E_i$$

$$E_1 > E_2 > \cdots > E_n$$

For electrons, muons and interacting and noninteracting hadrons, these measurable quantities differ in their mean and their distribution, therefore they can be used to separate different kinds of particles. Moreover the values obtained depend on the momentum of the particle. Since the ARGUS shower detector has cylindrical symmetry, the angle of incidence for a particle varies with its polar angle with respect to the beam axis (fig.1), hence E, E_i and n show in addition a dependence on the polar angle θ.

These relationships have been determined for the different particle species using a data set collected with the ARGUS detector. A clean sample of electrons at different energies is available from the reactions

$$e^+e^- \to e^+e^-$$
$$e^+e^- \to e^+e^-\gamma$$
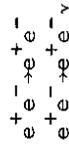
The electron momentum was measured in the drift chamber. A sample of muons of varying momenta was available from the processes

$$e^+e^- \to \mu^+\mu^-$$
$$e^+e^- \to \mu^+\mu^-\gamma$$
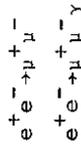
The muons have been identified with the muon chambers [5]. The sample of hadron tracks was taken from the data collected on the Υ-resonance, since the admixture of leptons for this data set is smallest. To suppress leptonic decay channels, events were used with more than ten neutral and charged particles. A small admixture of leptons due to weak decays of the hadrons is unavoidable for this data set, therefore the values for the separation powers given in this paper are lower limits. For hadron momenta smaller than 0.7 GeV/c, π- and K-mesons can be separated with the time of flight and the dE/dx systems, while protons and antiprotons are identified up to momenta of 1.2 GeV/c in the same manner.

III.1 Energy deposited by electrons in the shower counters

Since electrons deposit their total energy in the calorimeter, the electron momentum, as measured in the drift chamber, is a linear function of the energy detected by the shower counters (fig.2). The width of the distribution is determined by the resolution of the shower counters σ_E and the momentum resolution of the drift chamber, which has been measured to be

$$\frac{\sigma_p}{p} = 0.012 \cdot p$$

(p>1 GeV/c)

Adding these two contributions to the resolution quadratically

$$\sigma^2 = \sigma_p^2 + \sigma_E^2$$

a cut

$$|E - p \cdot c| \quad <N\sigma, \ N = 3, 4, \ldots$$

can be applied.

The dependence of the electron detection efficiency as a function of N is shown in fig. 3. For N=3 one obtains a detection efficiency of 86%. This is smaller than the expected value for a normal distribution because the two distribution functions are only approximately gaussian. The detection efficiency for a given N is approximately independent of momentum [8].

Since the electromagnetic shower has a finite spatial width and the particles in general traverse more than one shower counter, the energy deposited is spread over a cluster of neighbouring shower counters. In the analysis, only counters with an energy deposit larger than 10 MeV are taken into account to suppress background. For a given type of particle the mean number of shower counters hit (cluster size n) depends on the particle momentum and the polar angle of the incoming particle.

$$n = n (p,\theta)$$

A typical distribution of cluster size for the electron momentum interval of interest is shown in fig. 4a. The distribution has a large width due to the averaging over many impact directions and the inherent shower fluctuations. The mean cluster size increases linearly with the electron momentum, while its width is approximately constant (fig. 4b). The dependence of the cluster size on the polar angle is shown in fig. 4c for electrons with high momentum. The cluster size increases weakly with decreasing polar angle (fig.4c). The decrease observed at polar angles of $\theta \approx 45^{\circ}$ (ring 10,11) is due to the gap between the barrel and the end cap counters (fig.1).

III.2 _Energy deposition by muons in the shower counter_

Muons lose energy in the shower counters only by ionization and excitation processes. Normalizing the visible energy in the shower counter to the track length in the scintillator, one gets (fig. 5a) a mean energy loss per unit length of

$$\left\langle \frac{dE}{dx} \right\rangle = 2.4 \; \frac{MeV}{cm}$$

in good agreement with the expected value. The total energy deposited by muons in the shower counter is less than 500 MeV (fig. 5b). The cluster size as a function of the polar angle has a shape (fig. 5c) similar to the one for electrons, but the mean number of counters hit is smaller than 4 and therefore differs appreciably from the cluster size for electrons (fig. 4c).

From these observations it follows that a cut on the visible energy and on the cluster size is a powerful means of distinguishing between muons and electrons.

III.3 _Energy deposition of hadrons in the shower counters_

The energy deposited by hadrons in the shower counters is due to two processes. Noninteracting hadrons lose their energy by ionization and excitation. Hadrons that interact strongly initiate a hadron shower, whose energy is partially deposited in the shower counters. These two components can be clearly separated for particle momenta p≥2 GeV/c (fig. 6a). The visible energy in the shower counters has a pronounced peak at the position expected for minimum ionizing particles (fig. 6b). In addition, a broad continuum extends to high energies which is due to interacting hadrons. Cutting at an energy of 0.35 GeV approximately separates these two components. The measured cluster size of these two components shows the expected behaviour for minimum ionizing particles (fig. 7a) and interacting hadrons (fig. 7b) respectively. Moreover the distribution of the cluster size as a function of the polar angle for interacting hadrons is flat, while the dependence for noninteracting hadrons coincides with that measured for muons (fig. 5c). The fraction of interacting hadrons derived from figs. 6, 7 is (60.5±2.0)% and (50.4±1.9)% respectively; it is in agreement with the expected fraction of interacting hadrons derived from the interaction length of pions. The difference between the two results shows that cuts on the cluster size and the energy deposition don't result in clean samples of interacting and noninteracting hadrons.

Antiprotons in the momentum range of interest behave differently. Due to annihilation processes, they deposit an appreciable amount of their total energy in the shower counters. For anti-protons with p<1 GeV/c, the energy deposition and the cluster size are plotted in figs. 8a,b. Comparing figs. 8a,b and figs. 6a, 7b one observes a greater energy deposition and cluster size for the antiproton sample than for interacting hadrons. The cluster size depends strongly on the amount of energies deposited in the shower counters (fig. 8c). It should be noted that this dependence is steeper than for electrons. These observations can be exploited to enhance the fraction of anti-protons in the hadron sample.

IV. Particle separation with shower counters

In the previous section we have demonstrated that the energy deposition of different particle species shows distinct features. They can be used to separate electrons from hadrons and muons. Since hadrons loose their energy in the shower counter by two processes, the separation procedure has to handle these classes separately. The energy deposition of noninteracting hadrons agrees with that of muons, therefore the algorithm applied to this class of hadrons can best be demonstrated by comparing the energy loss of muons and electrons in the shower counters. The separation of muons and electrons is based mainly on the differences in the visible energy detected in the shower counters.
Interacting hadrons, on the other hand, initiate a hadronic shower which may deposit an amount of energy comparable to that of an electron with equal momentum. Therefore in this case more sophisticated methods, have to be applied.

IV.1 Electron-muon separation

The separation of electrons from muons and non-interacting hadrons is based on two observations. In fig. 5b it was shown that the energy loss of muons with p > 1 GeV/c is always smaller than 0.5 GeV, while electrons with these momenta are only accepted if their energy deposition is larger than 0.5 GeV. Furthermore the cluster-size for electrons and muons differs strongly (figs. 4c,5c). Cutting on the cluster size therefore allows one to detect electrons with high efficiency and to reject all muons. For particles with p>1 GeV/c a cut on the energy deposition (E>0.5 GeV/c) and on the cluster size (n>3) ensures a separation of electrons from minimal ionizing particles of over 500. The separation is defined as the probability of electrons passing the applied cuts to that of muons.

IV.2 Separation of electrons from interacting hadrons

The separation of showers induced by electrons from those induced by hadrons is based on two experimental observations. For electromagnetic showers the deposited energy E and the particle momentum p are strongly

correlated (fig. 4), while for hadrons no correlation is observed (fig. 9). A cut

$$|E-pc| < N\sigma$$

(N=3 or 4) already rejects an appreciable fraction of the hadrons while maintaining a detection efficiency (fig.3) for electrons of better than 86%. This procedure has also been applied in other experiments [6,7]. The rejection power depends on the resolution of the detector, with the best values having been attained with a BGO shower detector [6e].

In a second step we exploit the difference in the lateral energy spread of the showers initiated by eletrons and hadrons. The major fraction of energy for an electromagnetic shower is concentrated in a cone with a radius of a few millimeters, therefore 90% or more of the energy of an electron shower is deposited in the counter hit by the incoming particle (fig. 10, open circles), and only a small fraction of the total energy is shared by the neighbouring counters. Hadron induced showers (fig. 10 full circles) differ drastically from this behaviour. The deposited energy is shared by many neighbouring counters.

Starting from this observation we have developped an algorithm which allows one to separate electrons from interacting hadrons. To this end the lateral energy distribution for all showers with a cluster size n≥3 and an energy deposition E≥0.6 GeV/c is characterized by

$$\sigma_r^2 = \sum_{i=3}^{n} \frac{(\vec{r}_i - \vec{r})^2 E_i}{<r>^2}$$

where $\vec{r}_i$ = radius vector of the counter i
E_i = energy deposition in counter i with $E_1 \geq E_2 \geq \cdots \geq E_n$
$<r> \approx 10$ cm, average distance between the centers of two counters

$$\vec{r} = \frac{\sum_1^n E_i \vec{r}_i}{\sum_1^n E_i} \quad \text{radius vector of the cluster}$$

Note that the two counters with the highest energy deposition don't contribute to σ_r. The fractional width is defined by

$$f_{LAT} = \frac{\sigma_r^2}{\sigma_r^2 + E_1 + E_2}$$

with $0 \leq f_{LAT} \leq 1$. This variable can be used to separate electrons from hadrons as demonstrated in fig. 11a,b, where for electrons and hadrons respectively f_{LAT} is plotted as a function of the energy deposited in the shower counters. A clear difference between the two distributions exists for E ≥0.6 GeV. This is demonstrated in more detail in figs. 12a-c, where for three energy regions the f_{LAT} distributions for electrons (solid line) and hadrons (dotted line) are plotted. The distributions are normalized to the same area. The electron – hadron separation improves strongly with increasing momentum of the particles hitting the shower counters.

Different sets of cuts were applied to the data and their influence on the percentage of electrons and hadrons passing these cuts were studied (fig. 13). The results for the following three sets of cuts are especially instructive:

Set I.) clustersize n≥4 and $|E-p|<3\sigma$ (open triangles)
Set II.) Set I of cuts and E≥ 0.6 GeV, $f_{LAT} \leq a$ (ring number),
   where a is adjusted for each ring (fig.1) in such a way that
   5% of all electrons are rejected for the ring due to these
   cuts (full squares).
Set III.) Set I of cuts and E ≥1 GeV, $f_{LAT} \leq b$ (ring number), where
   b is adjusted such that 10% of all electrons are rejected
   for the corresponding ring due to these cuts (open circles).

The separate treatment of each ring is necessary since not only the clustersize (fig.4c,5c) but also the f_{LAT} distribution varies from one ring to another. To take this fact into account the detection efficiency of electrons (fig.13a) and hadrons (fig.13b) and the ratio of these efficiencies (fig.14a) (separation) was calculated by weighting the contribution of each ring in such a way that equal numbers of tracks from each ring are considered when calculating the respective variable.

The cut on the lateral shape of the energy distribution improves the separation by more than a factor 5 (fig.14a), while the separation for the set of cuts II and III respectively are equal within the error limits for the most interesting momentum interval p $\geq$1.5 $\frac{GeV}{c}$. The results for set II and III differ for low momentum electron (p$\leq$1.5 $\frac{GeV}{c}$). For the most interesting momentum interval for the experiment the separation of electrons and hadrons is larger than 50, while the electron detection efficiency exceeds 70%. The results for the barrel part of the shower counters (fig.1) are given separately in fig. 14b, the separation of electrons and hadrons is better than for the full detector. For momenta p $\geq$1.5 $\frac{GeV}{c}$ the electron and hadron efficiency are given separately in fig. 15 while the resulting separation is shown in fig. 16 as a function of the ring number. These plots demonstrate clearly the influence of the ring number on the separation. Thus a further improvement by a factor of 2 in the separation of electrons from hadrons can be achieved if one restricts the polar angle to the barrel region. This may be of interest if an very clean electron sample is needed.

The electron hadron separation attainable with the full ARGUS detector can be improved beyond the limits determined by the shower counters if one uses the energy loss of charged particles in the drift chamber [2]. In the drift chamber, electrons lose more energy than minimum ionizing particles (fig. 17). A combined cut on the shower counter information and the dE/dx signal as measured in the drift chamber results in an electron-hadron separation larger than 250.

V. Summary

The lateral shower energy deposition in the ARGUS electromagnetic calorimeter has been shown to have characteristic features which differ for electrons and hadrons. An algorithm has been developed which rejects hadrons with high probability (>50), while the electron detection efficiency is still larger than of 70%. The electron hadron separation power increases with the particle momentum.

The algorithm developed to separate electrons and hadrons on the basis of their lateral shower deposition turns out to be nearly as efficient as the one making use of the different longitudinal shower development of hadrons and electrons [6,7].

References

[1] ARGUS - A new detector for DORIS, DESY F15/PRO148/1978

[2] M. Danilov et al., Nucl.Instr.Meth. 217 (1983)153

[3] R.Heller et al., The ARGUS time of flight system, IHEP-HD/84-03, submitted to Nucl.Instr.Meth.

[4] a) W.Hofmann et al., Nucl.Instr.Meth.195(1982)475
   b) A.Drescher et al.,Nucl.Instr.Meth.205(1983)125
   c) A.Drescher et al.,Nucl.Instr.Meth.216(1983) 35
   d) J.Spengler, The ARGUS Electromagnetic Calorimeter System Proc. Intern.III Conference on Instrumentation for Colliding Beam Physics, Novosibirsk 1984 (in print)

[5] A.Arefiev et al., The ARGUS muon chambers DESY 83-025

[6] a) L.M.Ledermann et al., Nucl.Instr.Meth.129 (1975)65
   b) E.Gabathuler et al., Nucl.Instr.Meth.157 (1978)47
   c) J.H.Cobb et al., Nucl.Instr.Meth. 158 (1979)93
   d) A.Babaev et al., Nucl.Instr.Meth. 160 (1978)427
   e) H.Dietl et al., MPI-PAE/EXP.E1.124(1983)
   f) B.Cox et al., A measurement of the response of an SCG1-C Scintillation glass array to 4-14 GeV/c Pions, FNAL (1984)

[7] a) J.A.Appel et al., Nucl.Instr.Meth. 127(1975)495
   b) E.Locci et al., Nucl.Instr.Meth. 164(1979)97
   c) G.Battistoni, Proc.Intern.Conf. on Instr. for Colliding Beam Physics 1982, 195
   d) B.M.Bleichert et al., Particle Identification in an electron/hadron calorimeter Si-82-13

[8] B. Hahn, Diplomarbeit, Dortmund 1984

Figure Captions:

Fig. 1   Schematic view of the ARGUS detector
         1 drift chamber, 2 time of flight counters, 3 barrel shower counters, 4 end cap shower counters, 5 magnetic coil, 6 muon chambers, 7 iron yoke

Fig. 2   Energy E deposited in the shower counters versus momentum for electrons

Fig. 3   Percentage of electrons passing the cut $|E-p|<N\sigma$ as a function of N.

Fig. 4   a) Clustersize distribution for electrons (1 $GeV/c<p\leq2\,\frac{GeV}{c}$) hitting the shower counter
         b) Mean value of the clustersize versus electron momentum The error bars indicate the width of the clustersize distribution
         c) Mean clustersize as a function of the ring number, which is a measure of the polar angle of the particle

Fig. 5   a) Energy loss of muons per unit track length in the shower counters
         b) Total energy loss of muons in the shower counters
         c) Clustersize and width of muons, hitting the shower counters as a function of the ring number

Fig. 6   a) Energy deposited by hadrons in the shower counters
         b) Energy per unit track length deposited in the shower counters

Fig. 7   a) Clustersize distribution of noninteracting hadrons in the shower counters
         b) Clustersize distribution of interacting hadrons in the shower counters

Fig. 8   a) Energy deposited by antiprotons in the shower counters
         b) Clustersize distribution of antiprotons in the shower counters
         c) Clustersize versus energy distribution for antiprotons in the shower counters

Fig. 9   Energy deposited by hadrons in the shower counters versus momentum

Fig. 10   Fraction of the total shower energy deposited in the distance R from the impact point for electrons (open circles) and hadrons (full circles) depositing E≥0.6 GeV in the calorimeter

Fig. 11 f_{LAT} parameter defined in the text as a function of the energy E deposited in the shower counters for a) electrons and b) hadrons

Fig. 12   Distribution of f_{LAT} for electron (full line) and hadrons (broken line) for three energy intervals

          a) E ≥ 0.6 GeV,   b) E ≥ 1.0 GeV   c) E ≥ 1.5 GeV

Fig. 13   a) Electron detection efficiency and b) hadron detection efficiency as a function of the particle momentum for the full detector

          ▽ Set of cuts I (see text)
          ■ Set of cuts II(see text)
          ○ Set of cuts III (see text)

Fig. 14   Separation = electron detection efficiency/hadron detection efficiency for different particle momenta

          a) full shower detector   b) barrel shower counters (fig.1) The symbols are defined in fig.13

Fig. 15   Electron and hadron detection efficiency for particles with momentum 1.5 $\frac{GeV}{c}$ ≤p≤ 2.5 $\frac{GeV}{c}$ and the set of cuts III as a function of the ring number.

Fig. 16   Separation of electrons and hadrons for particles with momentum 1.5 $\frac{GeV}{c}$ ≤p≤ 2.5 $\frac{GeV}{c}$ as a function of the ring number.

Fig. 17 f_{LAT} versus dE/dx in the drift chamber for hadrons (right peak) and electrons (left peak) with momentum 1.5 $\frac{GeV}{c}$ ≤p≤2.5 $\frac{GeV}{c}$.
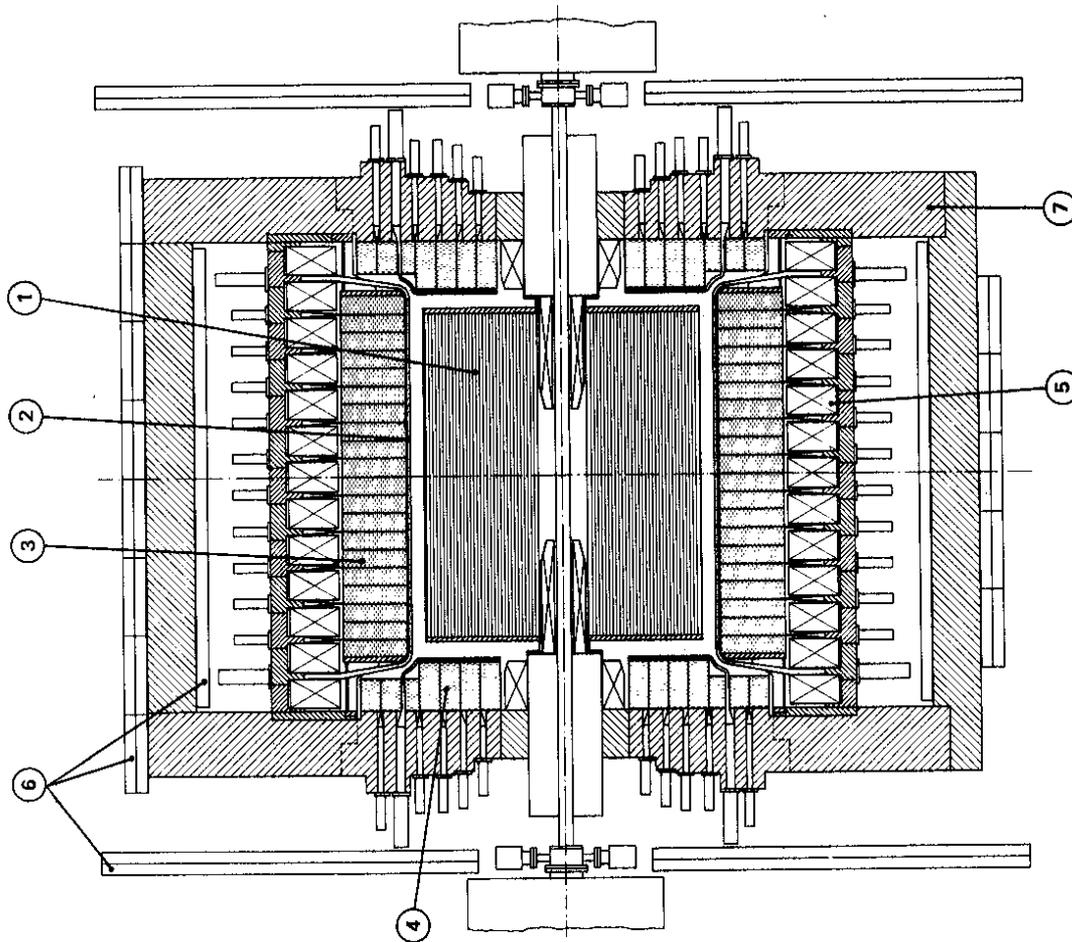
Fig. 1
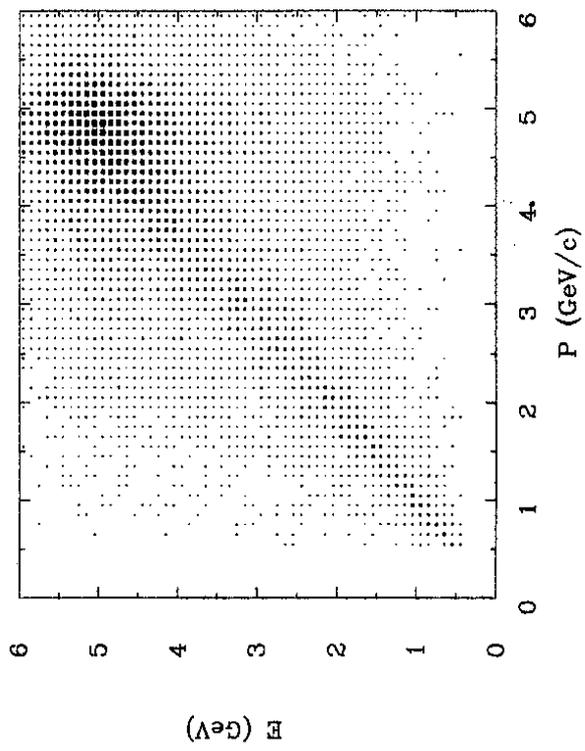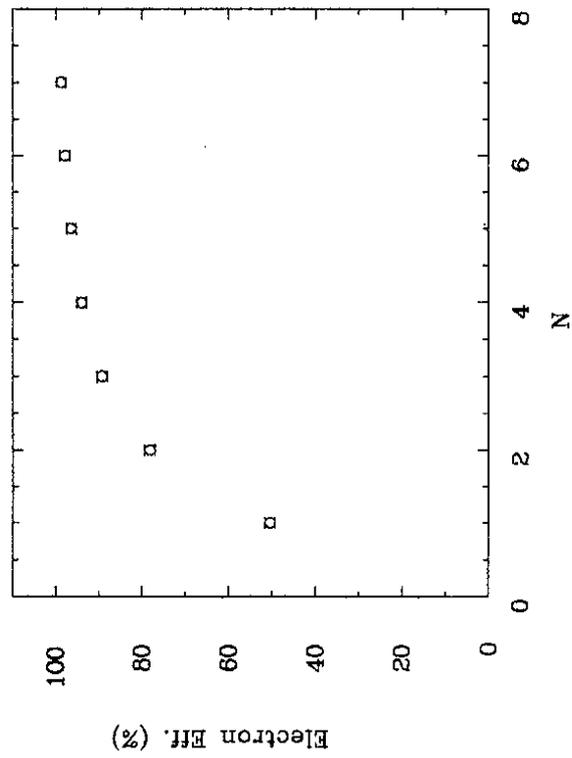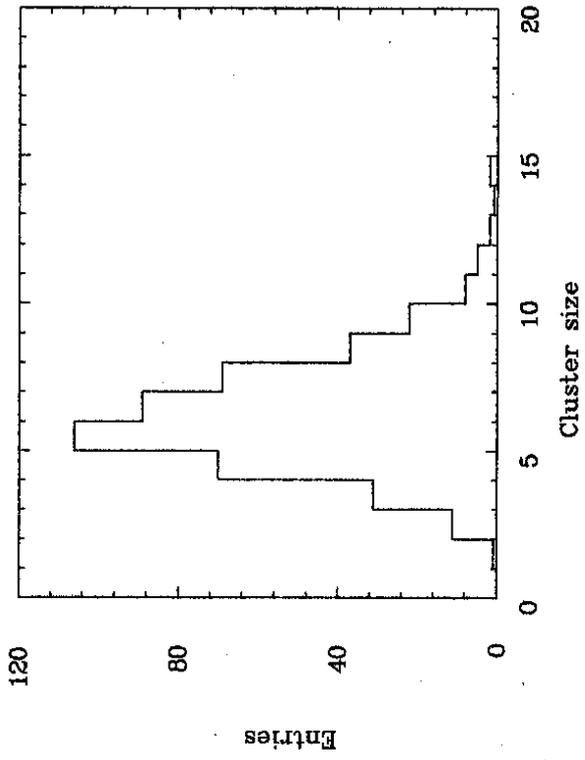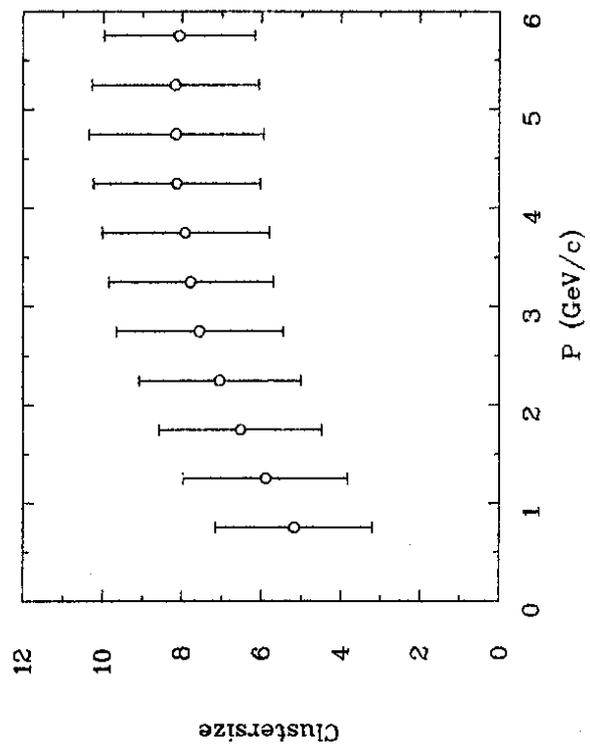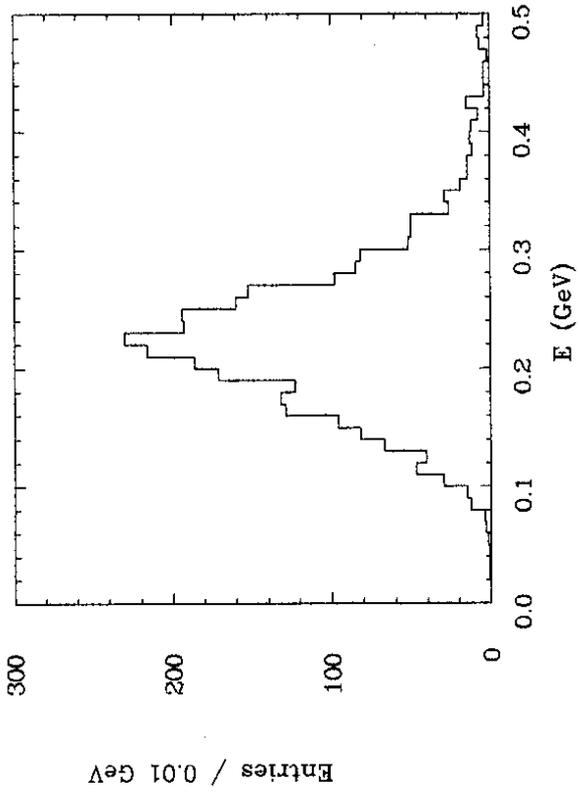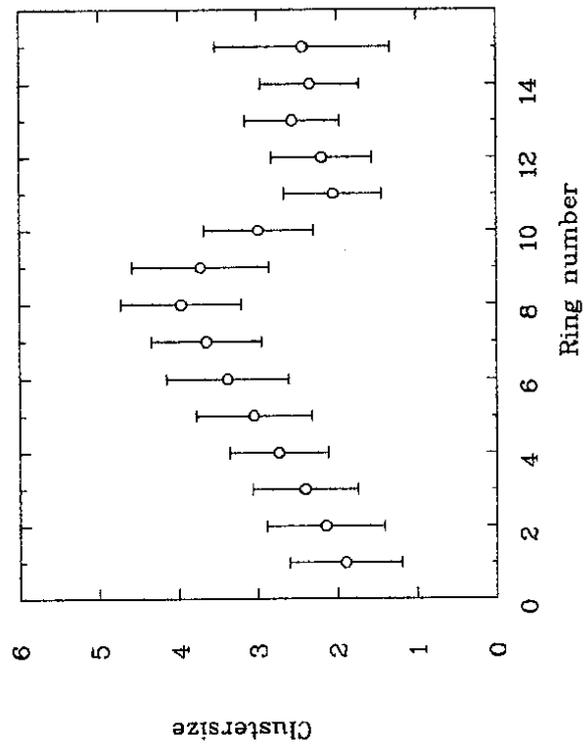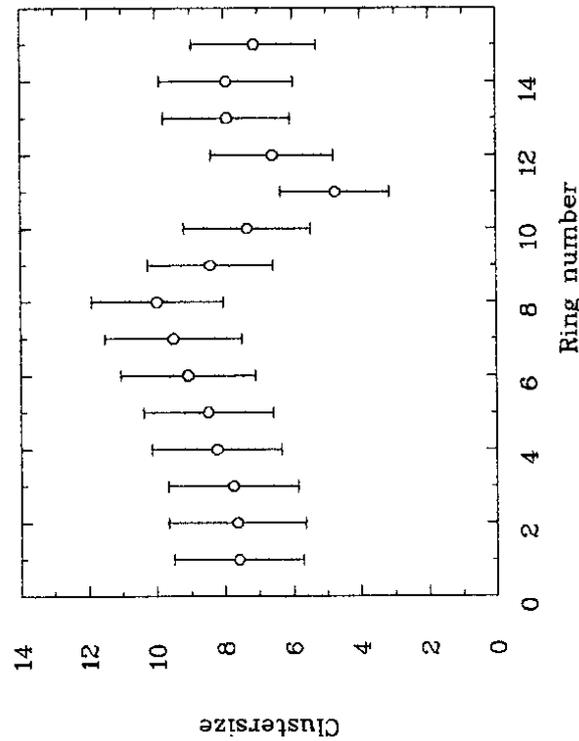
Entries

120

80

40

0

0   5   10   15   20

Cluster size

Fig. 4a

E (GeV)

6

5

4

3

2

1

0

0   1   2   3   4   5   6

P (GeV/c)

Fig. 2

Clustersize

12

10

8

6

4

2

0

0   1   2   3   4   5   6

P (GeV/c)

Fig. 4b

Electron Eff. (%)

100

80

60

40

20

0

0   2   4   6   8

N

Fig. 3

Entries / 0.01 GeV

300

200

100

0

0.0   0.1   0.2   0.3   0.4   0.5

E (GeV)

Fig. 5b

Clustersize

6

5

4

3

2

1

0

0   2   4   6   8   10   12   14

Ring number

Fig. 5c

Clustersize

14

12

10

8

6

4

2

0

0   2   4   6   8   10   12   14

Ring number

Fig. 4c

Entries / (0.2 MeV/cm)

400

300

200

100

0

0   1   2   3   4   5   6   7

dE/dx (MeV/cm)

Fig. 5a

Entries

Cluster size

Fig. 7a

Entries

Cluster size

Fig. 7b

Entries / 0.025 GeV

E (GeV)

Fig. 6a

Entries / (0.2 MeV/cm)

dE/dx (MeV/cm)

Fig. 6b

Fig. 8a

Fig. 8b

Fig. 8c

Fig. 9

f (LAT) (%)

E (GeV)

Fig. 11a

f (LAT) (%)

E (GeV)

Fig. 11b

E / ETOT (%)

R (cm)
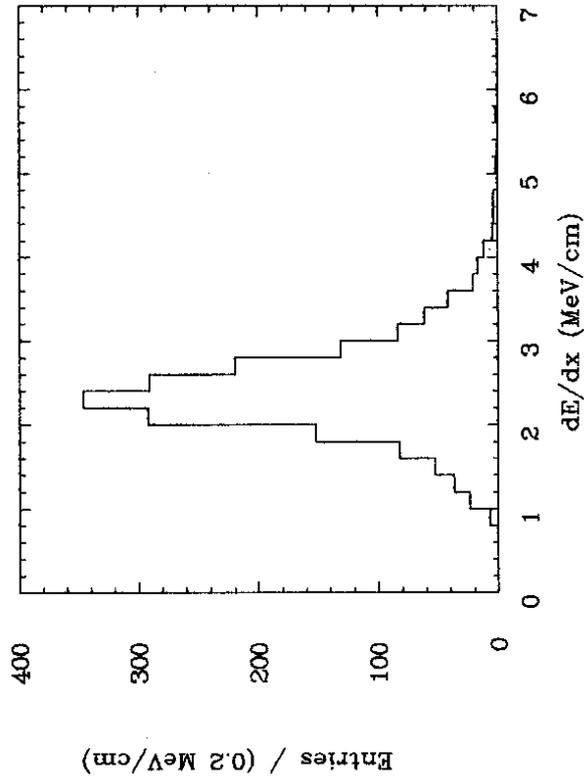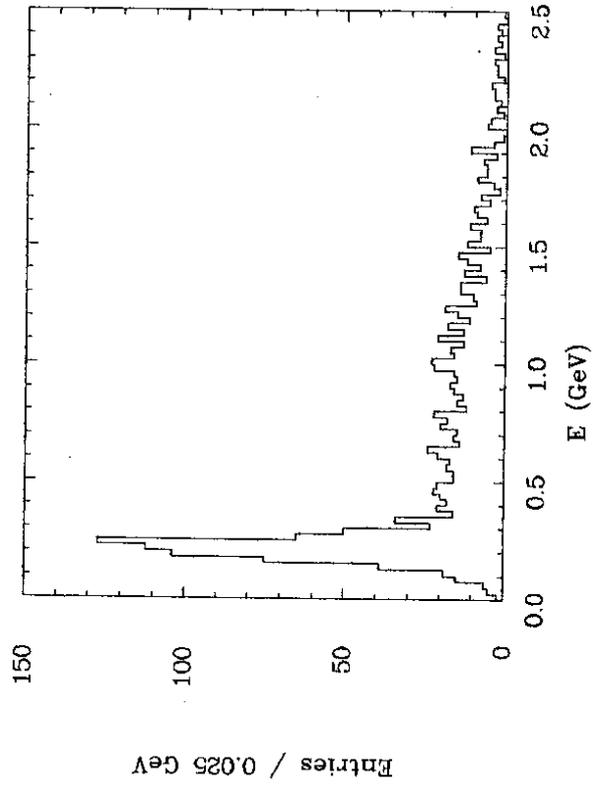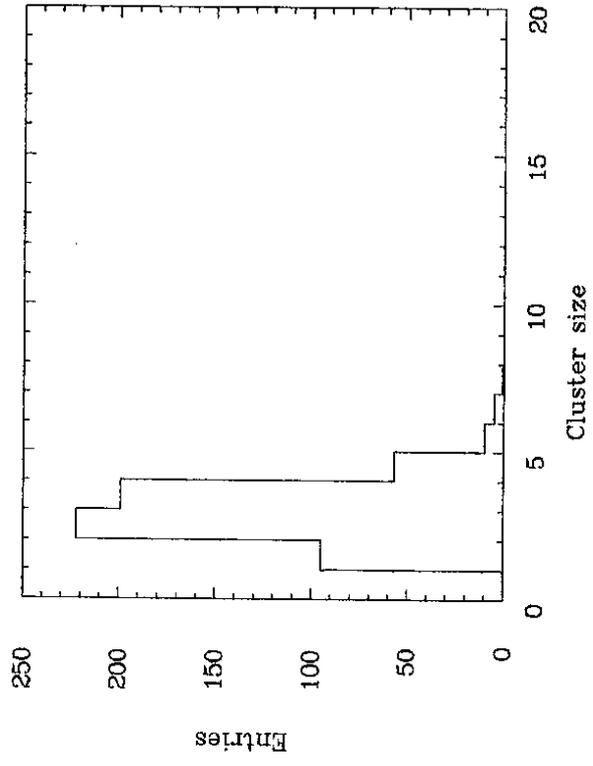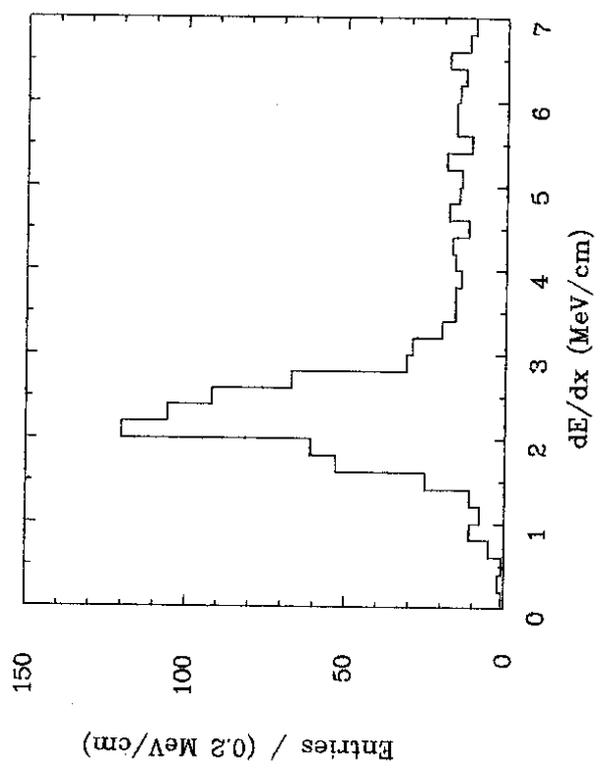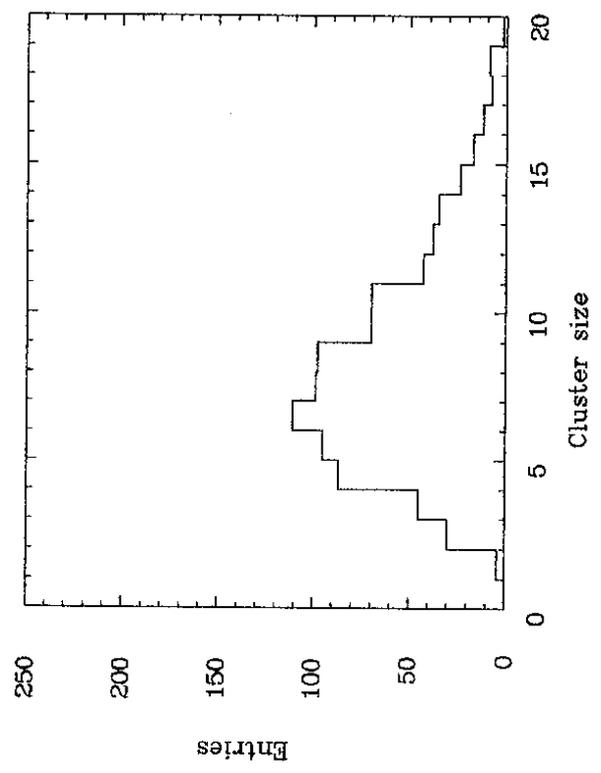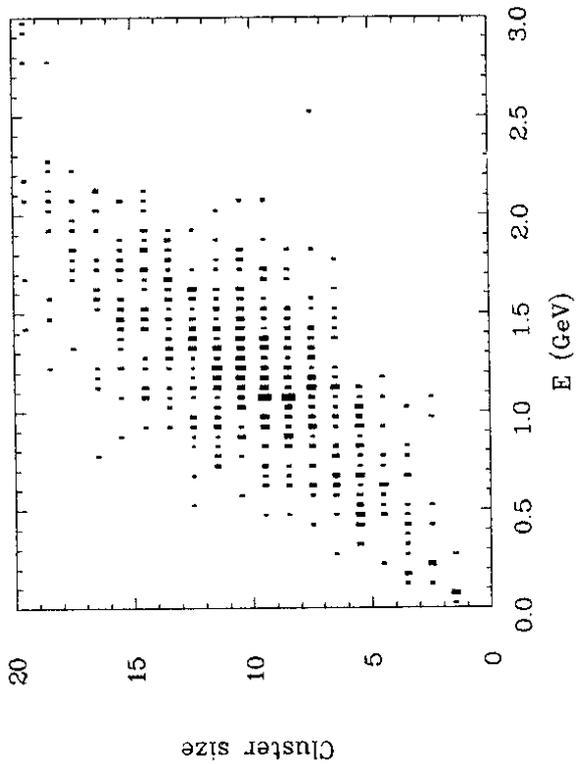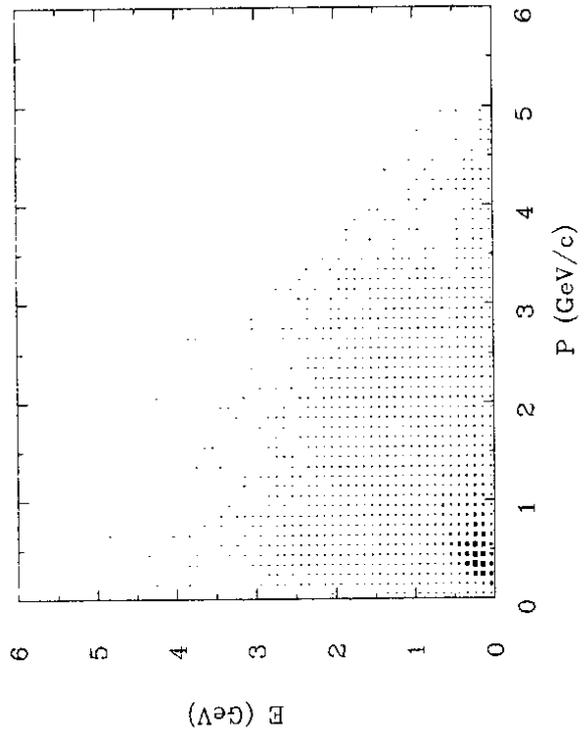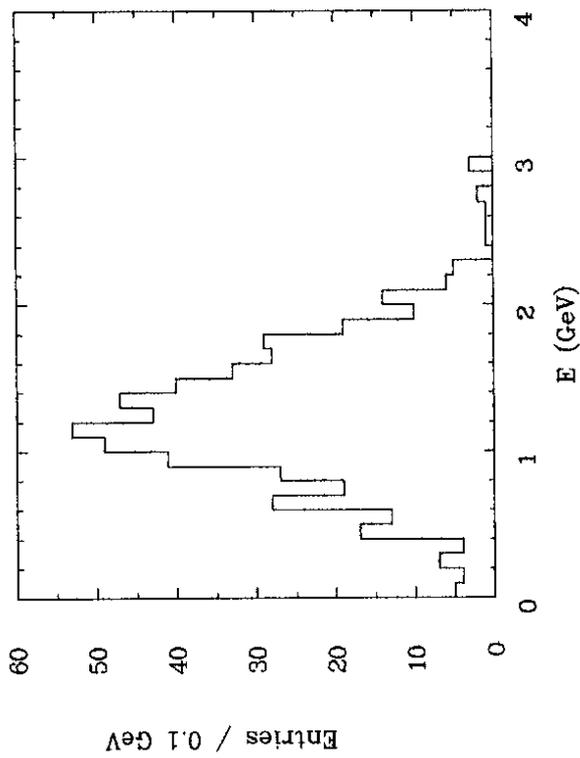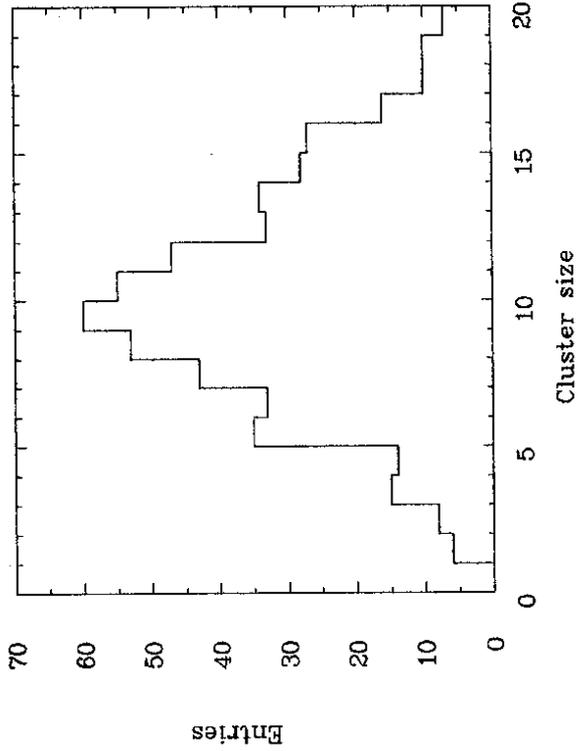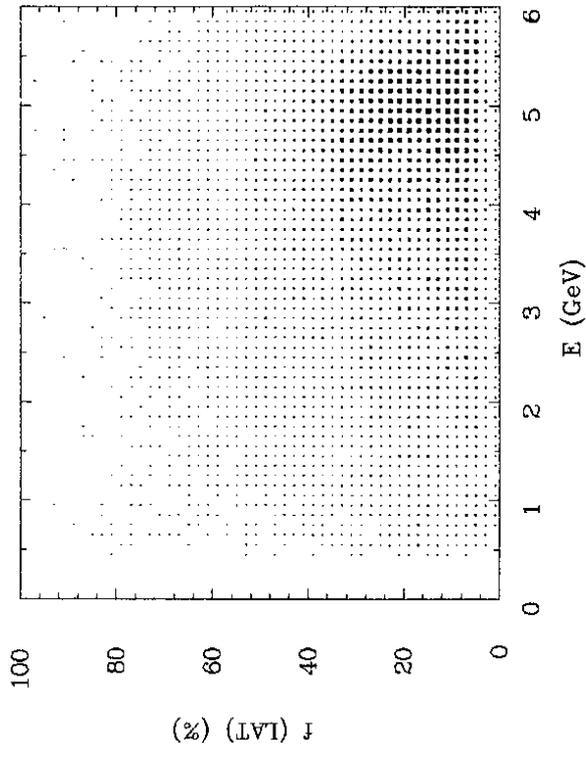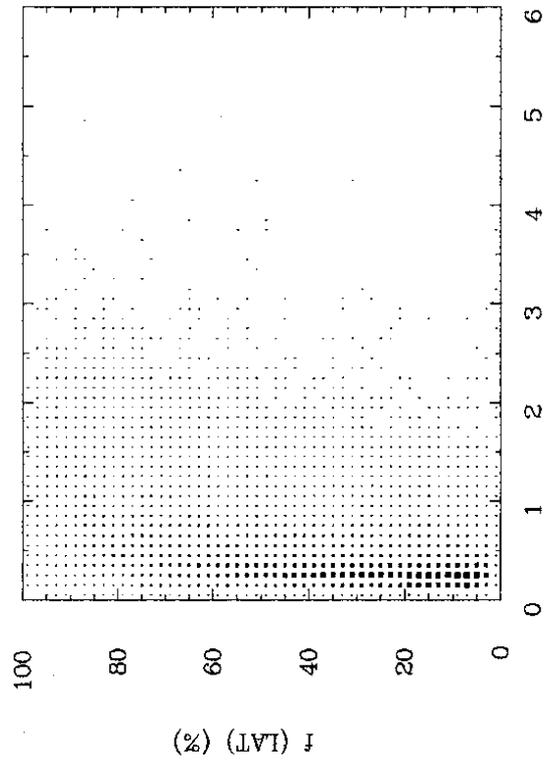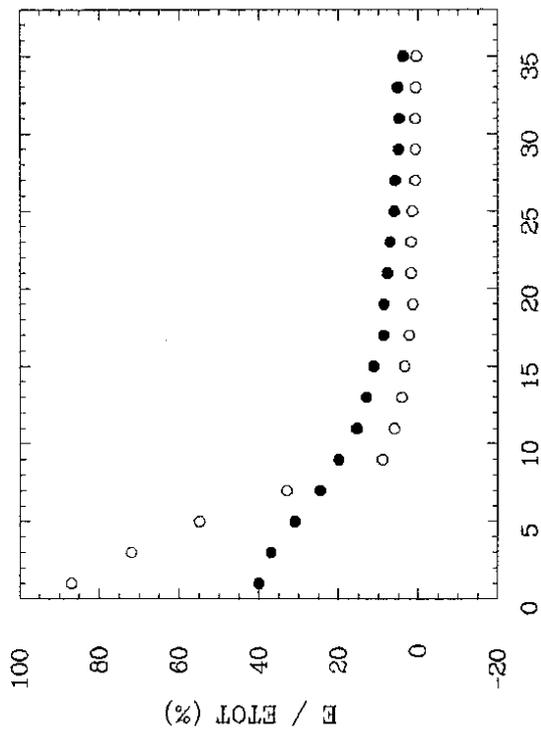
Fig. 10
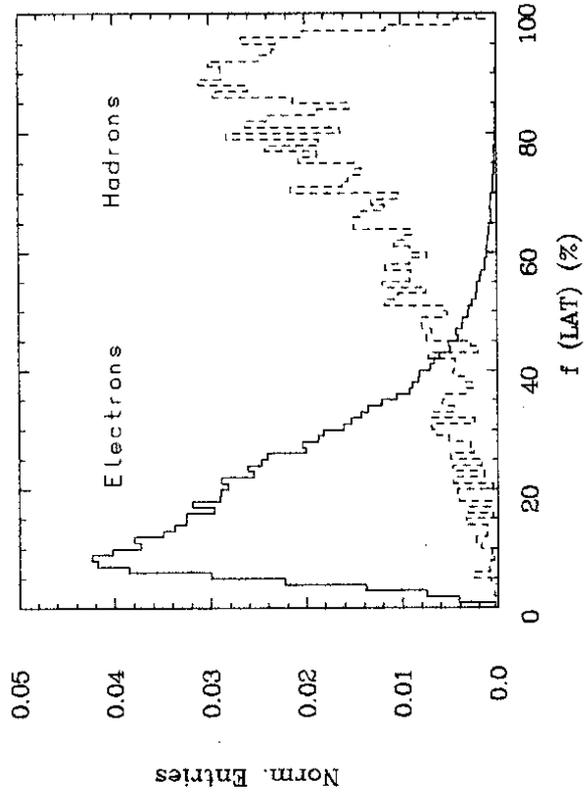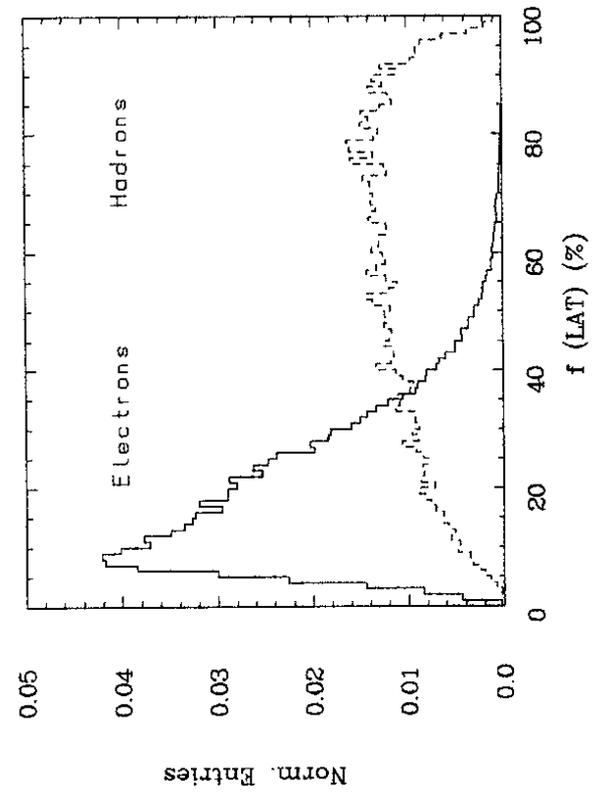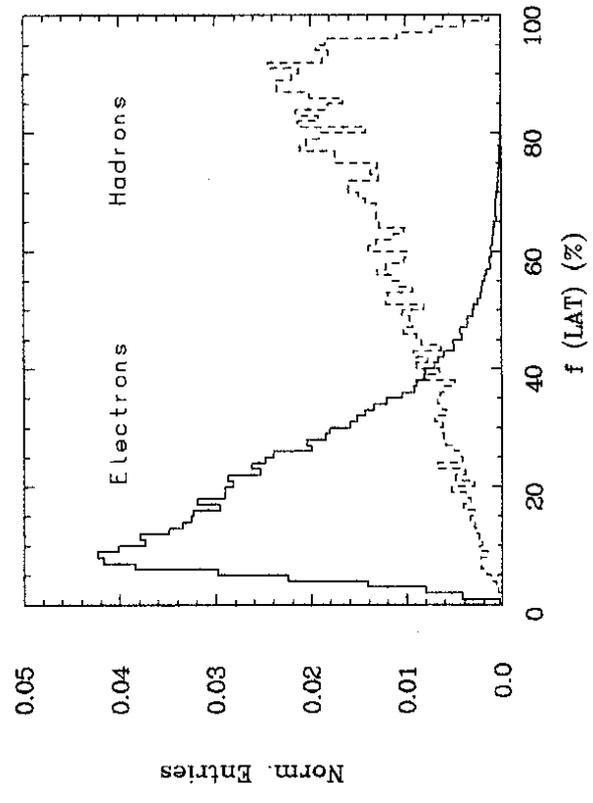
Fig. 12c

Fig. 12a

Fig. 12b
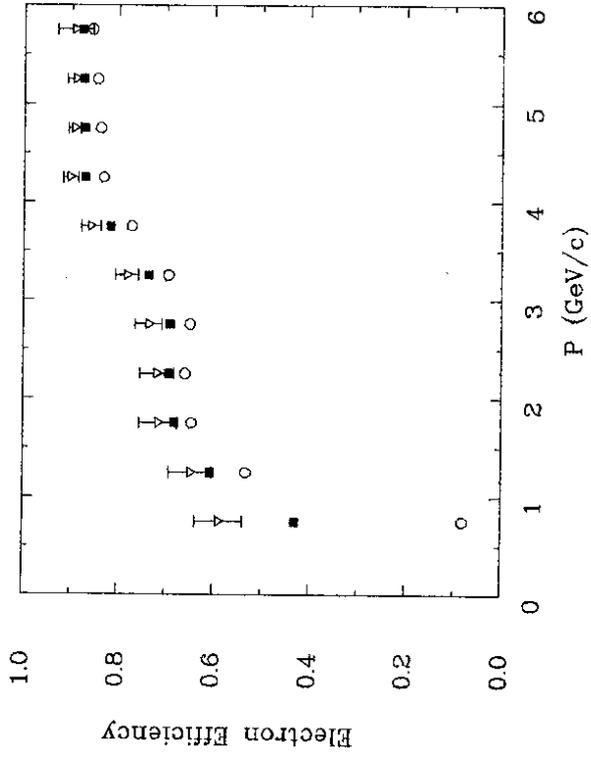
Fig. 13a
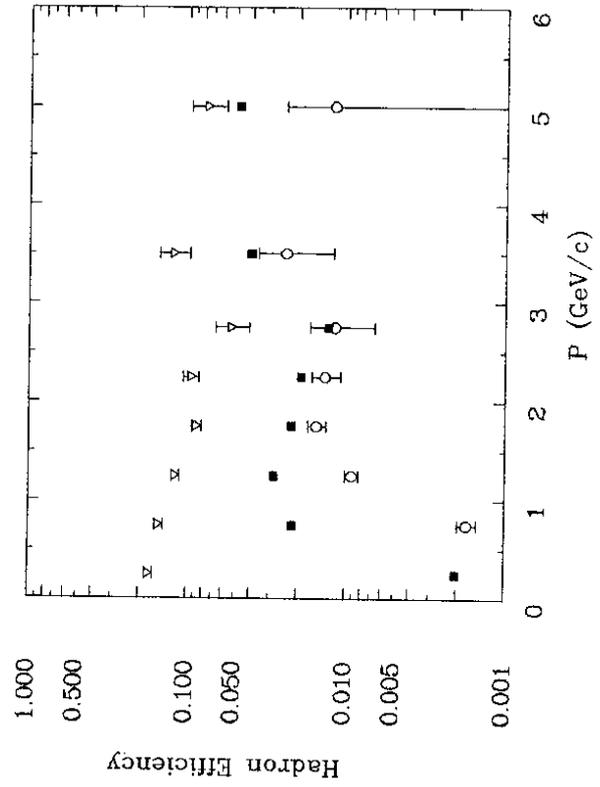
Fig. 13b

Fig. 14a

Fig. 14b

Fig. 17

Fig. 15

Fig. 16